

# A Semi-Analytical Model for InSb Crystal Growth

C. Sean Bohun\*, Ian Frigaard†, Huaxiong Huang‡ & Shuqing Liang§

July 21, 2003

## Abstract

In this paper we describe the basic idea of a semi-analytical approach for computing the temperature and thermal stress inside an Indium Antimonide (InSb) crystal grown with the Czochralski technique. An analysis of the growing conditions indicates that the crystal growth occurs on the conductive time scale. A perturbation method for the temperature field is developed using the Biot number as a (small) expansion parameter whose zeroth order solution is one-dimensional (in the axial direction) and is obtained for a cylindrical and a conical crystal. For the growth conditions of InSb a parabolic temperature profile in the radial direction is shown to arise naturally as the first order correction. As a result, the thermal stress is obtained explicitly and its magnitude is shown to depend on the zeroth order temperature and Biot number linearly. Some issues relevant to growth conditions are also discussed.

## 1 Introduction

The Czochralski method is the most popular technique for growing single large crystal used by the semiconductor and related industries. By dipping a small seed crystal into a pool of molten material in the crucible and carefully controlling the heat balance inside the grower, a large crystal can be grown by pulling the crystal away from the melt in a slow and steady fashion. The pulling rod and the crucible are normally rotated in the opposite directions during the growth period. Delicate control is often needed to maintain the crystal quality and a slight change of growth condition may result in defect formation inside the crystal. With care, a pure ('defects free') crystal can be obtained routinely when the size of the crystal does not exceed a critical size.

Due to the seemingly complex nature of the thermal, structural and dynamical coupling of the molten material, the crystal, the crucible, the gas chamber and other parts of the growth, considerable efforts have been devoted to the laboratory experiments and to modelling and simulations of the growth environment over the past several decades. As a result, there exist an extensive literature, mostly in engineering fields. These studies cover a wide spectral of areas, from decoupled one or two dimensional simulations to fully coupled three-dimensional computations [15, 16, 17, 18, 19, 20, 21]. Most of the studies rely heavily on computer simulation since the fully coupled system can not be solved otherwise. These investigations have generated useful information including temperature distribution, crystal-melt interface shape, and melt flow patterns inside the crucible. By comparison, until recently much less attention has been paid to the modelling of defects inside the crystal and main factors which determine the formation of defects [10].

In this paper, we present a semi-analytical approach to study the temperature field inside the crystal and related thermal stress. It is believed that the defects formation can be related to the excessive thermal stress above some critical value (see [3, 11, 12, 13, 14, 21, 22] and references therein). Therefore, some analysis on the growth factors which determine the stress level will be extremely useful for crystal growers using different operating conditions for less well-known crystals such as InSb.

---

\*Department of Mathematics, Pennsylvania State University, Mont Alto, PA 17237. [csb15@psu.edu](mailto:csb15@psu.edu)

†Department of Mathematics, University of British Columbia, Vancouver, BC V6T 1Z2. [frigaard@math.ubc.ca](mailto:frigaard@math.ubc.ca)

‡Department of Mathematics and Statistics, York University, Toronto, Ontario M3J 1P3. [hhuang@yorku.ca](mailto:hhuang@yorku.ca)

§Department of Mathematics and Statistics, York University, Toronto, Ontario M3J 1P3. [sqliang@mathstat.yorku.ca](mailto:sqliang@mathstat.yorku.ca)

The purpose of the paper is two-fold. By identifying the main physical features and using suitable mathematical models, we hope to gain further understanding of this complex manufacturing process. By deriving semi-analytical solutions, we also wish to provide useful insights which can be used to search for suitable growth conditions to improve the manufacturing procedure for InSb crystals.

By examining the physical process and parameter values of the growth environment closely, we are able to identify the main features associated with InSb crystals. In particular, we found that the temperature field is dominated by the lateral flux through the crystal-gas surface, characterized by the non-dimensional Biot number. The value of the Biot number is small under the growth condition for InSb crystals, which suggests an asymptotic expansion of the solution with respect to the Biot number. As a result, analytical solutions could be obtained for the pseudo-steady case, which is another main feature of the temperature field inside the crystal. This is similar to the growth of other crystals where the pseudo-steady assumption has been discussed in detail [23]. More detailed discussion related to the growth conditions for InSb will be given in Sections 2 and 5. Even for the fully unsteady case, the asymptotic expansion results in a system of one-dimensional equations and the thermal stress can be obtained explicitly in an analytical form, under the plane strain assumption. To simplify the presentation, we have used a simplified model for the melt and gas flows. However, the asymptotic solution developed here is still valid and can be incorporated with more realistic models for the melt and gas flows. Compared to most of the previous work, the results of this study are different since an explicit form for the stress is obtained. Formulated in a non-dimensional form, the dependence of the stress level on the Biot number is useful for crystal growers when larger crystals are grown. Since the Biot number is proportional to the product of the heat transfer coefficient and the mean crystal radius, it is obvious that one should try to reduce the heat flux via the lateral surface when a crystal of larger radius is grown.

The rest of the paper is organized as follows. In Section 2, we will present the mathematical model and dimensional analysis. Asymptotic solutions are given in Section 3. Thermal stress is discussed in Section 4. In Section 5, results are presented for both pseudo-steady and unsteady cases. We will conclude the paper with a brief summary and discussion on future directions in Section 6.

## 2 Mathematical Model and Dimensional Analysis

The overall aim of the paper is to derive a realistic but simplified model of InSb crystal growth. Figure 1 illustrates the profile of a typical crystal. The coordinate system is fixed to the top of the growing crystal at  $z = 0$  and the final length of the crystal is denoted  $Z$  and the crystal radius is denoted  $R(z)$ . The growth starts with a seed crystal with radius of order  $R_{\text{seed}} = 5 \times 10^{-3}$  m and length  $Z_{\text{seed}} = 3 \times 10^{-2}$  m. The crystal grows outwards in a slowly developing cone eventually reaching a radius  $R(Z) \simeq 5 \times 10^{-2}$  m, after a length  $Z \simeq 0.3$  m. A crystal can take 10-20 hours to grow. Thus, at the outset we observe firstly, that crystal growth is characterised by a large aspect ratio. Secondly, it is evident that any transients in the system, unless caused by rapidly changing boundary conditions, are very slow. These two features will be used to derive our eventual model.

Within the crystal  $\Omega$ , the temperature  $T(\mathbf{x}, t)$  satisfies the heat equation

$$\rho_s c_s \frac{\partial T}{\partial t} = k_s \sum_j \frac{\partial^2 T}{\partial x_j^2}, \quad \mathbf{x} \in \Omega, \quad t > 0 \quad (1)$$

where  $\rho_s$ ,  $c_s$  and  $k_s$  are the density, specific heat and thermal conductivity of the crystal, (i.e. the solid phase), respectively. The lateral surface of the crystal is denoted  $\Gamma_g$  and is subjected to cooling from the circulating chamber gases and radiative heat loss. Although radiation is not insignificant, for simplicity we model both effects through a simple Newtonian cooling law:

$$-k_s \frac{\partial T}{\partial \mathbf{n}} = h_{gs}(T - T_g), \quad \mathbf{x} \in \Gamma_g. \quad (2)$$

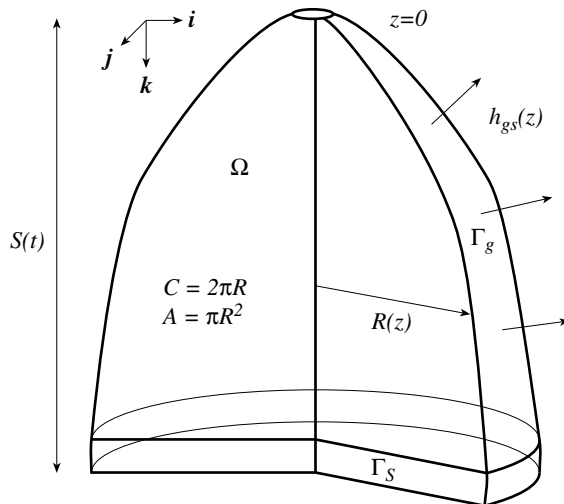


Figure 1: Shown is a typical crystal at some time  $t$  during a growth run with a newly solidified portion at  $z = S(t)$ . The coordinate system is chosen so that the top of the crystal remains at  $z = 0$  and the solidification front grows downwards in the positive  $z$  direction. The radial profile is given by  $R(z)$  and the crystal length is  $S(t)$ . Finally, the heat transfer coefficient  $h_{gs}(z)$  may be a function of the axial position  $z$ .

Here we assume that the heat transfer coefficient,  $h_{gs}$ , incorporates both convective and radiative heat transfer, (the latter via linearisation). The top of the crystal is fixed at  $z = 0$  where we also invoke a Newtonian cooling law

$$k_s \frac{\partial T}{\partial z} = h_{ch}(T - T_{ch}), \quad (3)$$

in the case that the radius at  $z = 0$  is assumed to be non-zero. Here  $h_{ch}$  represents the heat transfer coefficient for the seed-chuck connection and  $T_{ch}$  is the chuck temperature.

The crystal-melt interface is denoted  $\Gamma_S$  and is where  $T = T_s$ , the solidus temperature. The solidus isotherm is thus implicitly defined from the temperature field. Explicitly we denote the solidus isotherm by

$$z - S(\mathbf{x}, t) = 0, \quad \mathbf{x} \in \Gamma_S. \quad (4)$$

The motion of the solidus isotherm is governed by the Stefan condition

$$\rho_s L \frac{\partial S}{\partial t} = k_s \frac{\partial T}{\partial \mathbf{n}} \Big|_{z \rightarrow S^-} - q_l \quad (5)$$

where  $L$  is the latent heat and  $q_l$  is the heat flux from the melt. The speed  $\partial S / \partial t$  above is the speed at which the solidus moves in the direction of the outward normal  $\mathbf{n}$ . The Stefan condition can also be rewritten in terms of  $S(\mathbf{x}, t)$  for  $\mathbf{x} = (x, y)$ , as follows:

$$\rho_s L \frac{\partial S}{\partial t} = k_s \left( \frac{\partial T}{\partial z} - \frac{\partial S}{\partial x} \frac{\partial T}{\partial x} - \frac{\partial S}{\partial y} \frac{\partial T}{\partial y} \right) \Big|_{z \rightarrow S^-} - q_l.$$

## 2.1 Typical scales in InSb crystal growth

Although possible to treat the three-dimensional case above, it is somewhat unwieldy and hence we instead attempt to simplify the model first. Table 1 specifies a typical set of thermophysical and process data.

Data	Symbol	Value
Growing Properties		
Mean crystal radius	$\bar{R}$	0.03 m
Final crystal length	$Z$	0.30 m
Characteristic growth rate	$\bar{v}$	$3 \times 10^{-6}$ m/s
Ambient gas temperature	$T_g$	600 K
Solid Properties		
Solidus temperature	$T_s$	798.4 K
Density	$\rho_s$	$5.64 \times 10^3$ kg/m <sup>3</sup>
Thermal conductivity	$k_s$	4.57 W/m K
Heat capacity	$\rho_s c_s$	$1.5 \times 10^6$ J/m <sup>3</sup> K
Latent heat of fusion	$L$	$2.3 \times 10^5$ J/kg
Heat Transfer Coefficients		
Crystal-Gas	$h_{gs}$	1 – 4 W/m <sup>2</sup> K

Table 1: A summary of the thermophysical and typical growth parameters of InSb.

Consider a time  $t$ , after any initial growth transient, when the crystal has length  $S$  onto which a thin layer of crystal of radius  $\bar{R}$  has just solidified. Utilizing (1) and the characteristic values in Table 1, the conduction of heat across a crystal cross-section and the time taken to grow a length  $\bar{R}$  of crystal have the following time scales:

$$t_{\text{cond}} \simeq \frac{\bar{R}^2 \rho_s c_s}{k_s} = 3.0 \times 10^2 \text{ s}, \quad t_{\text{grow}} \simeq \frac{\bar{R}}{\bar{v}} = 1.7 \times 10^4 \text{ s}.$$

Thus, the conductive time scale is typically much shorter than that for growth, (i.e. over similar length-scales). The growth time scale for the entire crystal is still longer, and given by  $t \simeq Z/\bar{v}$ . It is over this latter growth time scale that significant changes in either the radius or area occur, which are related to significant changes in the cooling capacity and heat capacity, respectively.

Therefore, apart from imposed rapid changes in the growth, (e.g. at the start of the process and at the end as the crystal is withdrawn from the melt), all other thermal changes are slow and occur on the growth time scale. Since there is no process change that occurs on the conductive time scale, the process is likely to be pseudo-steady on the growth related time scale.

Turning now to the thermal gradients, the magnitude of the radial variation in the temperature is maximized at the lateral surface where the crystal comes into contact with the surrounding gas. From (2) and Table 1,

$$\left| \frac{\partial T}{\partial n} \right|_{\Gamma_g} \leq \frac{h_{gs}}{k_s} (T_s - T_g) \simeq 175 \text{ K/m}.$$

The magnitude of the axial temperature gradient is maximal at the solidus where the Stefan condition (5) is satisfied. Assuming a nearly flat interface (which will be justified later), an estimate for  $\partial T/\partial z|_{S^-}$  is obtained by neglecting the heat flux in the liquid phase:

$$\left| \frac{\partial T}{\partial z} \right|_{S^-} \simeq \frac{\rho_s L \bar{v}}{k_s} = 850 \text{ K/m}.$$

The sides of the crystal are predominantly vertical and the solidus isotherm predominantly horizontal. Thus, we see that the vertical gradients dominate, at least in some neighbourhood of the solidus isotherm. However, we must note that the vertical gradients arise mostly due to heat loss to the cooling gases, which occurs in the radial direction. Since the cooling effects are weak, this implies that a long crystal is needed to get a significant temperature drop along the crystal length and suggests that we will need to scale the axial and radial directions differently.

## 2.2 Non-dimensionalization

The above discussion motivates our scaling below. For simplicity, we start by assuming an axisymmetric model, although the crystal cross-section is not in fact circular. The other assumptions that we make here, for simplicity only, are that the heat transfer coefficient  $h_{gs}$  and the gas temperature  $T_g$  are constant. In reality there will be local variations along the crystal surface, but in any case these require a more detailed analysis of the gas flows in order to be properly evaluated.

We define the Biot number by

$$\epsilon = \frac{h_{gs}\bar{R}}{k_s} \quad (6)$$

and using the parameter values in Table 1, we find  $\epsilon \simeq 0.026 \ll 1$ . We seek an asymptotic expansion in terms of  $\epsilon$ . With this in mind we adopt the following scalings:

$$\begin{aligned} r &= \bar{R}\hat{r}, & \epsilon^{1/2}z &= \bar{R}\hat{z}, & R(z) &= \bar{R}\hat{R}(\hat{z}), & \epsilon^{1/2}S(r, t) &= \bar{R}\hat{S}(\hat{r}, \hat{t}), \\ T &= T_g + \Delta T\Theta, & \Delta T &= T_s - T_g, \\ t &= \frac{S_t\bar{R}^2\rho_s c_s}{k_s\epsilon}\hat{t}, & S_t &= \frac{L}{c_s\Delta T}. \end{aligned}$$

Here variables with hats ( $\hat{\cdot}$ ) are the non-dimensional ones. In terms of these variables the heat equation in the crystal (1) becomes

$$\frac{\epsilon}{S_t}\Theta_t = \frac{1}{r}(r\Theta_r)_r + \epsilon\Theta_{zz}, \quad \mathbf{x} \in \Omega, \quad t > 0 \quad (7)$$

with boundary conditions (2)-(4)

$$\begin{aligned} -\Theta_r + \epsilon\Theta_z R'(z) &= \epsilon[1 + \epsilon(R'(z))^2]^{1/2}\Theta, & \mathbf{x} &\in \Gamma_g, \\ \Theta &= 1, & \mathbf{x} &\in \Gamma_S, \\ \Theta_z &= \delta(\Theta - \Theta_{ch}), & z &= 0, \end{aligned} \quad (8)$$

where  $\delta = \epsilon^{1/2}h_{ch}/h_{gs}$ . The hats have been dropped for brevity. The solidus advances according to the Stefan condition (5) which in non-dimensional coordinates becomes

$$\Theta_z - \frac{1}{\epsilon}S_r\Theta_r = \left(1 + \frac{S_r^2}{\epsilon}\right)^{1/2}(\gamma + S_t), \quad (9)$$

where

$$\gamma = \frac{q_l}{\frac{\epsilon^{1/2}k_s\Delta T}{\bar{R}}}, \quad (10)$$

which is the non-dimensional heat flux in the liquid across the solidus. Note that we have chosen the rate of solidification to define the characteristic time scale. The Stefan number,  $S_t$ , gives the ratio of this characteristic solidification time scale to the time scale associated with conductive heat loss through the crystal side surface. Based on the parameter values in Table 1, we have  $S_t \approx 4.3$ , which suggests that the conductive scale is small and the temperature inside the crystal is steady on the growth time scale.

## 2.3 Growth Conditions

Under general growth conditions the process may be pseudo-steady. However, near the end of the process, transient effects may become important. To investigate both possibilities, this subsection describes two situations:

1. The growth of the crystal is characterized by an externally chosen value of  $q_l$  (or the non-dimensional flux  $\gamma$ ), constant for the duration of the simulation.

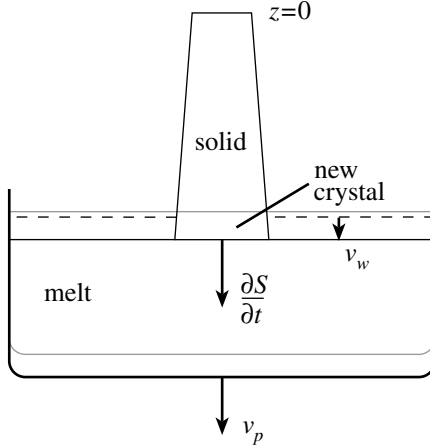


Figure 2: Shown here are the three velocities related to the extraction of the crystal. The crystal solidifies at a rate  $\partial S/\partial t$  and due to mass conservation, the surface of the fluid drops at a rate  $v_w$ . To ensure that the crystal melt interface remains at the surface of the liquid the crucible is dropped at a rate  $v_p$ . The three surfaces are, lighter line: old melt surface position; darker line: new melt surface position; broken line: melt level before extracting crystal (dropping crucible).

- Using the temperature of the furnace as a control parameter,  $q_l$  is determined implicitly by an effective heat transfer coefficient of the furnace to the crystal through the melt.

In the second scenario we use a simple model to couple the heat fluxes inside the grower based on the fact that system is almost at thermal equilibrium. Starting with dimensional variables, we consider crystal growth in an axisymmetric setting where the rate of growth is small. We assume that the melt (liquid) in the crucible is well-mixed and the temperature of the melt,  $T_l(t)$ , is uniform in space except in the thin layers near the crystal-melt and melt-ambient gas interfaces. We also assume that the ambient gas is well mixed and the temperature of the gas is a constant  $T_g$ . Furthermore, we will neglect the shape of meniscus and assume that the crystal-melt and gas-melt interfaces are flat.<sup>1</sup> Therefore by adjusting the pulling speed  $v_p$ , the positions of the crystal-melt and melt-gas interfaces can be described by a single function  $z = S(R, t)$ . Finally we assume that the crystal radius  $R(z)$  varies slowly in the  $z$  direction,  $|\partial R/\partial z| \ll 1$ . The coordinate system is fixed to the top of the growing crystal at  $z = 0$ , as described previously.

Let  $A = \pi R^2$  denote the cross sectional area of the crystal and  $A_c = \pi R_c^2$  be the cross section area of the crucible with  $R_c$  being the inside radius of the crucible at the current interface position. From the conservation of mass

$$\rho_l A_c v_w = \rho_s A \frac{\partial}{\partial t} S(R, t),$$

so that the rate at which the interface drops due to the change in density upon solidification is

$$v_w = \frac{\rho_s A}{\rho_l A_c} \frac{\partial}{\partial t} S(R, t)$$

resulting in a pull rate of

$$v_p = \frac{\partial S}{\partial t} - v_w = \frac{\rho_l A_c - \rho_s A}{\rho_l A_c} \frac{\partial}{\partial t} S(R, t).$$

<sup>1</sup>For InSb crystals under consideration here, the typical length scale is  $\bar{R}=0.03$  cm, the surface tension coefficient between the melt and gas is  $\sigma_{gl}=0.457$  (unit), and the melt density is  $\rho_l=6.47 \times 10^3$  kg/m<sup>3</sup>. The Bond number,  $Bo = \frac{\bar{R}^2 \rho_l g}{\sigma_{gl}} \simeq 10^4$ , is large. Thus the meniscus is dominated by the gravity effect and the meniscus only changes shape near the three-phase contact point with a small capillary rise.

This is detailed in Figure 2. Note that if the radius of the crystal is much smaller than the radius of the crucible  $A \ll A_c$  then  $v_w \simeq 0$ , or  $v_p \simeq \partial S / \partial t$ . If the actual pull rate of the crystal exceeds  $v_p$  by a moderate amount then the surface tension of the melt will cause the radius of the crystal to decrease. Similarly, pulling at a rate slower than  $v_p$  will cause the radius to increase.

Using these velocities, the position of the crystal-melt interface is  $S(t) = u_p(t) + u_w(t) + Z_{\text{seed}}$  where

$$u_p(t) = \int_0^t v_p(t) dt, \quad u_w(t) = \int_0^t v_w(t) dt$$

are the displacements due to the growth of the crystal and the loss of melt during the solidification respectively. Assuming the crucible is initially full, the depth of the crucible,  $Z_c$ , is also the initial depth of the melt.

During the growth period, the heat balance inside the melt yields

$$\frac{d}{dt} (\rho_l c_l T_l V_l) = -q_l A + (A_c - A) h_{gl} (T_g - T_l) + A_l h_{cl} (T_c - T_l), \quad T_l(0) = T_s,$$

where  $q_l = h_{sl}(T_l - T_s)$ ,  $\rho_l$  and  $c_l$  are the density and specific heat of the melt,  $V_l$  is the total volume of the melt,  $T_s$  is the melting/solidification temperature, and  $h_{sl}$  and  $h_{gl}$  are the heat transfer coefficients between the melt-crystal and melt-ambient gas respectively. The last term is the heat flux from the crucible to the liquid, which is assumed to be a control parameter with the temperature of the crucible  $T_c$  as the control parameter. Here  $A_l$  is the area of the crucible covered by the melt and  $h_{cl}$  is the heat transfer coefficient between the melt and the crucible. Since the shape of the crucible is known,  $A_l$  and  $V_l$  can be obtained as

$$A_l = \int_0^{Z_{c0} - u_w(t)} 2\pi R_c(\xi) (1 + R_c'(\xi))^2 d\xi, \quad V_l = \int_0^{Z_{c0} - u_w(t)} \pi R_c^2(\xi) d\xi.$$

These integrals are computed with respect to a local coordinate system fixed to the bottom of the crucible, which will be used for the rest of this section.  $Z_{c0}$  is the height to which the crucible should be filled so that once the crystal reaches its final mass, and the growth stops, there is a given proportion,  $p$ , of melt mass left in the crucible. This condition can be expressed as

$$\frac{\rho_s}{\rho_l} V_{\text{xtal}} = (1 - p) \int_0^{Z_{c0}} \pi R_c^2(\xi) d\xi.$$

By defining

$$\lambda = \frac{\bar{R}}{\bar{R}_c}, \quad \mu = \frac{\bar{R}_c}{Z_c}, \quad \phi = \frac{\rho_l c_l}{\rho_s c_s}, \quad \beta = \frac{\lambda^3 \bar{R}_c}{\epsilon^{1/2} Z_c}$$

substituting

$$\begin{aligned} A &= \bar{R}^2 \hat{A}, & R_c &= \bar{R}_c \hat{R}_c, & A_c &= \bar{R}_c^2 \hat{A}_c, & A_l &= \bar{R}_c Z_c \hat{A}_l, \\ V_l &= \bar{R}_c^2 Z_c \hat{V}_l, & Z_{c0} &= Z_c \hat{Z}_{c0}, & \epsilon^{1/2} u_p &= \bar{R} \hat{u}_p, & \epsilon^{1/2} u_w &= \lambda^3 \bar{R}_c \hat{u}_w, \\ T_l &= T_g + \Delta T \Theta_l, & T_c &= T_g + \Delta T \Theta_c, \end{aligned}$$

and dropping hats one obtains the following heat balance expression

$$\frac{\phi}{S_t} \frac{d}{dt} \left[ \left( \frac{T_g}{\Delta T} + \Theta_l \right) V_l \right] = \mu \lambda^3 \frac{h_{sl}}{h_{gs}} A (1 - \Theta_l) - \mu \lambda \frac{h_{gl}}{h_{gs}} (A_c - \lambda^2 A) \Theta_l + \lambda \frac{h_{cl}}{h_{gs}} A_l (\Theta_c - \Theta_l), \quad \Theta_l(0) = 1 \quad (11)$$

with geometric factors

$$A_l = \int_0^{Z_{c0} - \beta u_w(t)} 2\pi R_c(\xi) (1 + \mu^2 R_c'(\xi))^2 d\xi, \quad V_l = \int_0^{Z_{c0} - \beta u_w(t)} \pi R_c^2(\xi) d\xi, \quad (12)$$

melt surface displacements

$$u_w(t) = \int_0^t \frac{\rho_s A}{\rho_l A_c} \frac{\partial}{\partial t} S(R, t) dt, \quad u_p(t) = S(R, t) - S(R, 0) - \lambda^2 u_w(t), \quad (13)$$

and velocities

$$v_w = \frac{\rho_s A}{\rho_l A_c} \frac{\partial}{\partial t} S(R, t), \quad v_p = \left(1 - \lambda^2 \frac{\rho_s A}{\rho_l A_c}\right) \frac{\partial}{\partial t} S(R, t). \quad (14)$$

This implies the relationship  $v_p = \partial S / \partial t - \lambda^2 v_w$  at  $r = R$ . For this second scenario equation (10) becomes

$$\gamma = -\epsilon^{1/2} \frac{h_{sl}}{h_{gs}} (1 - \Theta_l). \quad (15)$$

### 3 Perturbation solution

We now seek to approximate the scaled model in Section 2.2 via a straightforward perturbation expansion. In turn, this perturbation model will form the basis for a numerical solution. Since  $S_t$  is neither small nor too large under the current growth conditions it is retained as a parameter. Equations (7) & (8) strongly suggest that the temperature  $\Theta$  is independent of  $r$  to leading order. If true then the solidus isotherm  $S$  is also independent of  $r$  to leading order, and we see that this is consistent in (9) with the growth being driven primarily by the vertical gradients. These observations motivate the following approximations:

$$\begin{aligned} \Theta &\sim \Theta_0(z, t) + \epsilon \Theta_1(r, z, t) + \epsilon^2 \Theta_2(r, z, t) + \dots \\ S &\sim S_0(t) + \epsilon S_1(r, t) + \epsilon^2 S_2(r, t) + \dots \end{aligned} \quad (16)$$

We substitute them into the scaled model, expand in powers of  $\epsilon$ , simplify and collect terms. The resulting field equations to first order are:

$$\frac{1}{S_t} \Theta_{0,t} = \frac{1}{r} \frac{\partial}{\partial r} (r \Theta_{1,r}) + \Theta_{0,zz}, \quad \mathbf{x} \in \Omega, \quad t > 0, \quad (17)$$

$$\frac{1}{S_t} \Theta_{1,t} = \frac{1}{r} \frac{\partial}{\partial r} (r \Theta_{2,r}) + \Theta_{1,zz}, \quad \mathbf{x} \in \Omega, \quad t > 0, \quad (18)$$

where the boundary condition on the lateral surface becomes

$$\Theta_{1,r} - R' \Theta_{0,z} = -\Theta_0, \quad r = R(z), \quad (19)$$

$$\Theta_{2,r} - R' \Theta_{1,z} + \frac{1}{2} R'^2 \Theta_0 = -\Theta_1, \quad r = R(z). \quad (20)$$

Continuing this procedure for the remaining conditions, at the top of the crystal one has

$$\begin{aligned} \Theta_{0,z} &= \delta(\Theta_0 - \Theta_{ch}), & z &= 0, \\ \Theta_{1,z} &= \delta\Theta_1, & z &= 0, \end{aligned}$$

and at the solid-liquid interface

$$\begin{aligned} \Theta_0 &= 1, & z &= S_0(t), \\ S_1 \Theta_{0,z} + \Theta_1 &= 0, & z &= S_0(t). \end{aligned}$$

Finally, the evolution of the interface is governed by

$$\gamma + S_{0,t} = \Theta_{0,z} \Big|_{z=S_0(t)}, \quad S_0(0) = Z_{\text{seed}}, \quad (21)$$

$$S_{1,t} = \left( \Theta_{1,z} + S_1 \Theta_{0,zz} + \frac{1}{2} \frac{\Theta_{1,r}^2}{\Theta_{0,z}} \right) \Big|_{z=S_0(t)}, \quad S_1(r, 0) = 0. \quad (22)$$

We note that  $Z_{\text{seed}}$  is the non-dimensional length of the seed. In addition there will be symmetry conditions at  $r = 0$  for  $\Theta_k, S_k, k = 0, 1$ .

### 3.1 Resolution of the zeroth order model

Integrating (17) once and imposing the symmetry condition  $\Theta_{1,r} = 0$  at  $r = 0$ , we have:

$$\frac{r}{2} \left( \frac{1}{S_t} \Theta_{0,t} - \Theta_{0,zz} \right) = \Theta_{1,r},$$

and applying (19) at  $r = R$  gives the zeroth order problem:

$$\frac{1}{S_t} \Theta_{0,t} = \Theta_{0,zz} + \frac{2}{R} (R' \Theta_{0,z} - \Theta_0), \quad 0 < z < S_0(t), \quad t > 0, \quad (23)$$

$$\Theta_{0,z} = \delta(\Theta_0 - \Theta_{ch}), \quad z = 0, \quad (24)$$

$$\Theta_0 = 1, \quad z = S_0(t) \quad (25)$$

where the advance of  $S_0(t)$  is coupled to the thermal gradients via (21).

Equation (23) is parabolic and involves only the heat fluxes along the length of the crystal. With the chosen expansion we see that at zeroth order the temperature field has no radial dependence. In addition, we can see that the thermal gradients, as discussed previously, are caused by cooling effects at the surface. In Section 5.1 we solve the time dependent system (21), (23)-(25) on  $(0, S_0(t))$  for a suitable set of initial conditions. Also notice that expression (21) illustrates that the chosen time scale balances the growth. The resultant appearance of  $1/S_t < 1$  in (23) suggests that thermal transients in the bulk of the crystal are not as important as the growth transient. Although this is explored further in Section 5.1, the limit at  $S_t \rightarrow \infty$  leads naturally to a pseudo-steady leading order model, in which time dependency only enters the thermal model through the growth, i.e. we also solve:

$$\Theta_{0,zz} + \frac{2}{R} (R' \Theta_{0,z} - \Theta_0) = 0, \quad 0 < z < S_0(t) \quad (26)$$

with the boundary conditions (24) & (25) with the growth of  $S_0(t)$  given by (21) as the pseudo-steady limit.

We note that properly it is necessary to close the model by relating growth in  $S$  to that in  $R$ . To do this we must model the crystal withdrawal from the crucible, formation of the meniscus in the holm region and coupling of  $S$  and  $R$ . It has been shown in [9] that the growth angle is related to the capillary height for large Bond number growth. In principle, crystals with desirable shapes can be grown by adjusting the pulling rate. Therefore, to simplify the computation, we impose a geometry  $R(z)$  on the model. This approach has the advantage of allowing us to investigate the thermal fields and associated stresses that develop for a particular observed shape. We start by exploring two special cases for which an analytic solution may be computed to the pseudo-steady model.

#### 3.1.1 Constant radius crystals

In this case we take  $R(z) = 1$  and (26) becomes simply

$$0 = \Theta_{0,zz} - 2\Theta_0, \quad 0 < z < S_0(t)$$

with boundary conditions (24) & (25). Solving for  $\Theta_0$  gives:

$$\Theta_0(z) = \frac{\sqrt{2} \cosh \sqrt{2}z + \delta \sinh \sqrt{2}z + \delta \Theta_{ch} \sinh \sqrt{2}(S_0 - z)}{\sqrt{2} \cosh \sqrt{2}S_0 + \delta \sinh \sqrt{2}S_0}. \quad (27)$$

The crystal grows at a rate governed by the Stefan condition (21):

$$\gamma + S_{0,t} = \sqrt{2} \frac{\sqrt{2} \sinh \sqrt{2}S_0 + \delta \cosh \sqrt{2}S_0 - \delta \Theta_{ch}}{\sqrt{2} \cosh \sqrt{2}S_0 + \delta \sinh \sqrt{2}S_0}.$$

We consider the following two limits:

- *Insulated chuck* ( $\delta = 0$ ):

$$\begin{aligned}\Theta_0(z) &= \frac{\cosh \sqrt{2}z}{\cosh \sqrt{2}S_0}, \\ \gamma + S_{0,t} &= \sqrt{2} \tanh \sqrt{2}S_0.\end{aligned}$$

- *Cold chuck* ( $\Theta_{ch} = 0$ ):

$$\begin{aligned}\Theta_0(z) &= \frac{\sqrt{2} \cosh \sqrt{2}z + \delta \sinh \sqrt{2}z}{\sqrt{2} \cosh \sqrt{2}S_0 + \delta \sinh \sqrt{2}S_0}, \\ \gamma + S_{0,t} &= \sqrt{2} \frac{\delta \cosh \sqrt{2}S_0 + \sqrt{2} \sinh \sqrt{2}S_0}{\sqrt{2} \cosh \sqrt{2}S_0 + \delta \sinh \sqrt{2}S_0}.\end{aligned}$$

### 3.1.2 Conical crystals

One source of ambiguity in the constant radius model above is the need to specify the chuck temperature and heat transfer coefficient. In the case of a conical crystal, (which is closer to reality), this ambiguity is less prominent. We assume  $R(z) = R_{\text{seed}} + \alpha z$  where  $\alpha \simeq O(1)$  is one-half the opening angle of the crystal when using non-dimensional units. In this case we solve

$$\left. \begin{aligned} 0 = \Theta_{0,\eta\eta} + \frac{2}{\eta}(\Theta_{0,\eta} - \Theta_0), \\ \Theta_{0,\eta} = \alpha\delta(\Theta_0 - \Theta_{ch}), \\ \Theta_0 = 1, \end{aligned} \right\} \begin{aligned} R_{\text{seed}} < \alpha^2\eta < R_{\text{seed}} + \alpha S_0, \quad t > 0, \\ \alpha^2\eta = R_{\text{seed}}, \\ \alpha^2\eta = R_{\text{seed}} + \alpha S_0, \end{aligned} \quad (28)$$

where  $\alpha^2\eta(z) = R_{\text{seed}} + \alpha z$ . In this case the solution takes the form of linear combinations of modified Bessel functions

$$\Theta_0(\eta, t) = \frac{g(\eta) [f'(\eta_0) - \alpha\delta f(\eta_0) + \alpha\delta\Theta_{ch}f(\eta_{S_0})] - f(\eta) [g'(\eta_0) - \alpha\delta g(\eta_0) + \alpha\delta\Theta_{ch}g(\eta_{S_0})]}{[f'(\eta_0)g(\eta_{S_0}) - f(\eta_{S_0})g'(\eta_0)] + \alpha\delta[f(\eta_{S_0})g(\eta_0) - f(\eta_0)g(\eta_{S_0})]} \quad (29)$$

where

$$\eta_0 = \eta(0), \quad \eta_{S_0} = \eta(S_0), \quad f(\eta) = \frac{I_1(\sqrt{8\eta})}{\sqrt{\eta}}, \quad g(\eta) = \frac{K_1(\sqrt{8\eta})}{\sqrt{\eta}}$$

and

$$f'(\eta) = \frac{\sqrt{2}}{\eta} I_0(\sqrt{8\eta}) - \frac{I_1(\sqrt{8\eta})}{\eta^{3/2}}, \quad g'(\eta) = -\frac{\sqrt{2}}{\eta} K_0(\sqrt{8\eta}) - \frac{K_1(\sqrt{8\eta})}{\eta^{3/2}}.$$

The corresponding expression for the growth rate is

$$\gamma + S_{0,t} = \frac{1}{\alpha} \frac{g'(\eta_{S_0}) [f'(\eta_0) - \alpha\delta f(\eta_0) + \alpha\delta\Theta_{ch}f(\eta_{S_0})] - f'(\eta_{S_0}) [g'(\eta_0) - \alpha\delta g(\eta_0) + \alpha\delta\Theta_{ch}g(\eta_{S_0})]}{[f'(\eta_0)g(\eta_{S_0}) - f(\eta_{S_0})g'(\eta_0)] + \alpha\delta[f(\eta_{S_0})g(\eta_0) - f(\eta_0)g(\eta_{S_0})]}$$

Two limiting cases are considered. To compare with the cylindrical case one sets  $R_{\text{seed}} = 1$  and expands (29) in a power series of  $\alpha$  yielding

$$\Theta_0(z, t) = \frac{\cosh \sqrt{2}z}{\cosh \sqrt{2}S_0} \left\{ 1 - \frac{\alpha}{8} \left[ 6(z - S_0) + \sqrt{8}(z^2 - U) \tanh \sqrt{2}z - \sqrt{8}(S_0^2 - U) \tanh \sqrt{2}S_0 \right] \right\} + \mathcal{O}(\alpha^2)$$

with

$$U = \frac{3}{2} + 2\delta \left( 1 - \Theta_{ch} \cosh \sqrt{2}S_0 \right)$$

which should be compared to equation (27). Since  $R_{\text{seed}} \ll 1$ , a simple form of (29) can be obtained by expanding the solution in  $R_{\text{seed}}$ , as

$$\Theta_0(z, t) = \sqrt{\frac{S_0}{z}} \frac{I_1(\sqrt{8z/\alpha})}{I_1(\sqrt{8S_0/\alpha})} \left[ 1 + \frac{R_{\text{seed}}}{\alpha} \left( \sqrt{\frac{2}{\alpha z}} \frac{I_0(\sqrt{8z/\alpha})}{I_1(\sqrt{8z/\alpha})} - \sqrt{\frac{2}{\alpha S_0}} \frac{I_0(\sqrt{8S_0/\alpha})}{I_1(\sqrt{8S_0/\alpha})} - \frac{1}{z} + \frac{1}{S_0} \right) \right] + \mathcal{O}(R_{\text{seed}}^2).$$

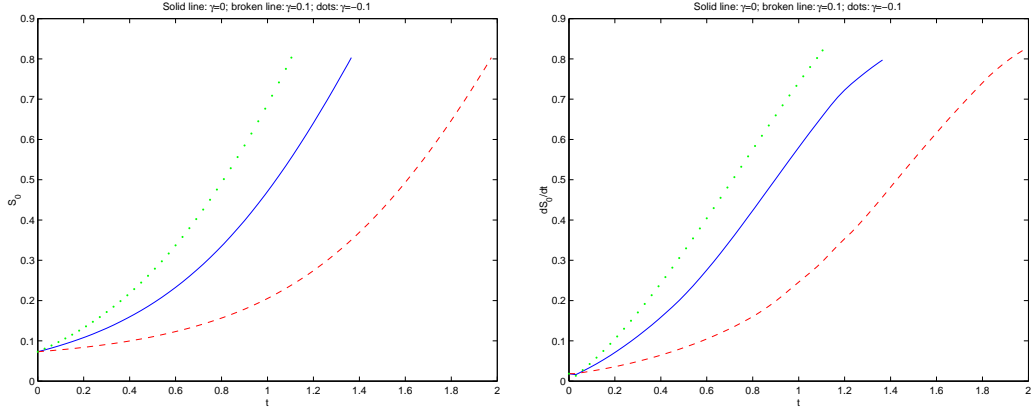


Figure 3: Effect of  $\gamma$  on growth of cylindrical crystals.

### 3.1.3 Comments

We note that the model for a one-dimensional temperature variation in the axial direction is not new. For example, it has been used in [9] as the model allows for simple analytical solutions. However, the model has not been formally justified in the crystal growth literature.

From the explicit solutions for cylindrical crystals one can observe that the rate of interface growth (therefore the rate of crystal growth) is asymptotically (for large  $S_0$ )  $\sqrt{2} - \gamma$ , when  $\gamma$  is constant. For small  $S_0$ , on the other hand, the speed is approximately  $4S_0 - \gamma$  for insulated chunk or  $\delta - \gamma$  for a cold chunk. This suggests, for both cases, that initially a small  $\gamma$  is necessary to establish the growth. In addition, the value of  $\gamma$  will also affect the total time required for growing crystals of certain sizes. We have experimented with the value of  $\gamma$ , in Figure 3  $S_0$  and its time derivative are plotted for three different  $\gamma$  values. The effect of  $\gamma$  is obvious.

The solution for conical crystals is more complicated and we will defer the discussion to Section 5.

## 3.2 Radial variations: resolution of the first order model

Having solved the zeroth order model, to give  $\Theta_0$  and  $S_0$ , we can resolve the radial variations in temperature which occur at first order in  $\Theta_1$  and also consider the shape of the solidus as it evolves, through  $S_1$ . From resolution of the zeroth order model we have that

$$\Theta_{1,r} = \frac{r}{2} \left( \frac{1}{S_t} \Theta_{0,t} - \Theta_{0,zz} \right),$$

which integrates with respect to  $r$  to give

$$\Theta_1(r, z, t) = \Theta_1(0, z, t) + \frac{r^2}{4} \left( \frac{1}{S_t} \Theta_{0,t} - \Theta_{0,zz} \right),$$

or

$$\Theta_1(r, z, t) = \Theta_1^0(z, t) + r^2 \Theta_1^1(z, t), \quad (30)$$

where  $\Theta_1^0(z, t) = \Theta_1(0, z, t)$  and using equation (23)

$$\Theta_1^1(z, t) = \frac{1}{2R(z)} (R'(z) \Theta_{0,z}(z, t) - \Theta_0(z, t)). \quad (31)$$

Note that the function  $\Theta_1^1(z, t)$  is known from the data and the zeroth order solution. By adopting the same procedure as for the zeroth order model we can find  $\Theta_1^0(z, t)$ , i.e. integrating (18) with respect to  $r$  and using the boundary condition at  $r = R$  to eliminate  $\Theta_{2,r}$ . We derive:

$$\frac{1}{S_t}\Theta_{1,t}^0 - \Theta_{1,zz}^0 - \frac{2}{R}(R'\Theta_{1,z}^0 - \Theta_1^0) = -\frac{R^2}{2}\left(\frac{1}{S_t}\Theta_{1,t}^1 - \Theta_{1,zz}^1\right) + 2R(R'\Theta_{1,z}^1 - \Theta_1^1) - \frac{R'^2}{R}\Theta_0, \quad (32)$$

$$\Theta_1^0(z, 0) = 0, \quad 0 < z < S_0(t), \quad (33)$$

$$\Theta_{1,z}^0 = \delta\Theta_1^0, \quad z = 0, \quad (34)$$

$$\Theta_1^0(z, t) = -S_1^0(t)\Theta_{0,z}(z, t), \quad z = S_0(t) \quad (35)$$

where  $S_1^0(t) = S_1(0, t)$  and its value is determined by the Stefan condition (22) at  $r = 0$  as

$$S_{1,t}^0 = (\Theta_{1,z}^0 + S_1^0\Theta_{0,zz})_{z=S_0(t)}, \quad S_1^0(0) = 0. \quad (36)$$

The evolution of the interface shape is governed by (22) which reduces to

$$S_{1,t} = \left[ \Theta_{1,z}^0 + S_1\Theta_{0,zz} + r^2 \left( \Theta_{1,z}^1 + \frac{2(\Theta_1^1)^2}{\Theta_{0,z}} \right) \right]_{z=S_0(t)}, \quad S_1(r, 0) = 0 \quad (37)$$

in which  $r$  appears as a parameter.

We note that (32)-(37) has the same structure as the zeroth order problem (21), (23)-(25), but is inhomogeneous, i.e. the zeroth order solution provides the forcing (or heating). A further key difference is in the coupling with the solidus position  $S_1$ . Equation (35) provides the lower boundary condition for  $\Theta_1$  and  $S_1$  advances through (37), which is consequently a first order pseudo-linear partial differential equation.

In general, the coupled system (32)-(37) must be solved numerically. For the pseudo-steady case, the formula can be simplified as follows.

From the definition of  $\Theta_1^1$  and using the pseudo-steady condition  $\Theta_{0,zz} = -4\Theta_1^1$  reduces expressions (32) & (37) to

$$\Theta_{1,zz}^0 + \frac{2}{R}(R'\Theta_{1,z}^0 - \Theta_1^0) = \frac{1}{4}(-RR''' + 5R'R'' + 2R')\Theta_{0,z} - \frac{1}{4R}(5RR'' - 4R'^2 + 2R)\Theta_0 \quad (38)$$

and

$$S_{1,t} = \left[ \Theta_{1,z}^0 + \frac{2}{R}(1 - R'\Theta_{0,z})S_1 + \frac{r^2}{2R^2} \left( R' + (RR'' - 2R'^2 - R)\Theta_{0,z} + \frac{1}{\Theta_{0,z}} \right) \right]_{z=S_0(t)}. \quad (39)$$

### 3.2.1 Constant radius crystals

Here  $R(z) = 1$  and  $\Theta_{0,zz} = 2\Theta_0$ . From the definition of  $\Theta_1^1$  we have

$$\Theta_1^1 = \frac{1}{2R}(R'\Theta_{0,z} - \Theta_0) = -\frac{1}{2}\Theta_0$$

giving  $\Theta_{1,z}^1 = -\Theta_{0,z}/2$  and  $\Theta_{1,zz}^1 = -\Theta_0$ . Consequently (38) becomes

$$\Theta_{1,zz}^0 - 2\Theta_1^0 = -\frac{1}{2}\Theta_0.$$

Solving for  $\Theta_1^0$  in the case that  $\delta = 0$  yields

$$\Theta_1^0 = \frac{1}{4\sqrt{2}} \frac{\cosh \sqrt{2}z}{\cosh \sqrt{2}S_0} \left( S_0 \tanh \sqrt{2}S_0 - z \tanh \sqrt{2}z - 8S_1^0 \tanh \sqrt{2}S_0 \right)$$

from which  $S_1$  can be obtained with equation (37).

### 3.2.2 Conical crystals

Here  $R(z) = R_{\text{seed}} + \alpha z$  and we have

$$\Theta_1^1 = \frac{1}{2R}(R'\Theta_{0,z} - \Theta_0) = \frac{1}{2R}(\alpha\Theta_{0,z} - \Theta_0)$$

with the identity  $\Theta_1^1 = -\Theta_{0,zz}/4$  from (26). Using these we derive

$$\Theta_{1,z}^1 = -\left(\frac{3\alpha^2}{2R^2} + \frac{1}{2R}\right)\Theta_{0,z} + \frac{3\alpha}{2R^2}\Theta_0, \quad \Theta_{1,zz}^1 = \left(\frac{6\alpha^3}{R^3} + \frac{3\alpha}{R^2}\right)\Theta_{0,z} - \left(\frac{6\alpha^2}{R^3} + \frac{1}{R^2}\right)\Theta_0$$

and finally simplify (38) to:

$$\Theta_{1,zz}^0 + \frac{2\alpha}{R}\Theta_{1,z}^0 - \frac{2}{R}\Theta_1^0 = \frac{\alpha}{2}\Theta_{0,z} + \frac{1}{2R}(2\alpha^2 - R)\Theta_0. \quad (40)$$

In general numerical methods will have to be used to find a solution to either case above. Even for the pseudo-steady solution. Further discussion is deferred to Section 5. In the following we turn our discussion to thermal stress inside the crystal.

## 4 Thermal Stress

The thermal stress experienced by the crystal during its growth leads to the generation of structural defects in the crystal [8]. If we want to eliminate these undesirable defects then one must control the thermal stress. We begin with a brief introduction to the case of an isotropic body. Although InSb is anisotropic with respect to its elasticity, this will be dealt with in a subsequent section.

### 4.1 Fundamentals

Consider the crystal as an isotropic body with deformations due to both a body force  $\vec{b}$  and changes in temperature. In general the temperature changes could be either a result of the deformation itself or applied through an external source. The un-deformed state of the body in the absence of body forces is associated with the ambient temperature  $T_g$ . In this case the expression for the stress tensor,  $\sigma_{ik}$ , of the deformed body is given by [7]

$$\sigma_{ik} = \frac{E}{(1+\nu)}u_{ik} + \frac{E\nu}{(1+\nu)(1-2\nu)}u_{ll}\delta_{ik} - \frac{E\alpha_0(T-T_g)}{(1-2\nu)}\delta_{ik} \quad (41)$$

where we have once again begun with the dimensional form of (41) to clarify the concepts. In this expression,  $T - T_g$  denotes the increment of the temperature over the reference temperature  $T_g$  and  $u_{ik}$  is the strain tensor defined as

$$u_{ik} = \frac{1}{2}\left(\frac{\partial u_i}{\partial x_k} + \frac{\partial u_k}{\partial x_i}\right) = \frac{1}{2}(u_{i,k} + u_{k,i}).$$

Notice that  $\sigma_{ik}$  is a  $3 \times 3$  symmetric matrix and as such has three real eigenvalues counting multiplicities. These eigenvalues are denoted  $\sigma_1$ ,  $\sigma_2$  and  $\sigma_3$  and if  $\sigma_{ik}$  is diagonal, the eigenvalues are simply the diagonal elements. In addition,  $E$  is the Young's modulus,  $\nu$  is the Poisson's ratio, and  $\alpha_0$  is the coefficient of thermal expansion of the given material. The quantities  $E$ ,  $\nu$  and  $\alpha_0$  are assumed to be constant since any allowance for their temperature dependence would lead to correction terms of higher order. Assuming that  $E$  is constant will tend to overestimate the amount of stress that is predicted. The overall behaviour of the stress will also be affected, but to a lesser extent.

Substituting the above expression for  $\sigma_{ik}$  into Cauchy's first law of motion,  $\sigma_{ik,k} + \rho b_i = \rho a_i$ , results in the equilibrium equation

$$\nabla(\nabla \cdot \vec{u}) - \frac{(1-2\nu)}{2(1-\nu)}\nabla \times \nabla \times \vec{u} = \frac{\alpha_0(1+\nu)}{(1-\nu)}\nabla T - \frac{(1+\nu)(1-2\nu)}{E(1-\nu)}\rho(\vec{b} - \vec{a}) \quad (42)$$

which defines the displacement vector  $\vec{u}$  where  $\rho$  is the mass density,  $\vec{b}$  is the body force per unit mass and  $\vec{a}$  is the acceleration vector of an element of the body.

Once the displacement vector has been determined the components of the strain tensor are simply various combination of derivatives. In cylindrical coordinates  $(r, \theta, z)$  with  $\vec{u} = \langle u, v, w \rangle$  one has [4]

$$\begin{aligned} u_{rr} &= \frac{\partial u}{\partial r}, & u_{\theta\theta} &= \frac{1}{r} \frac{\partial v}{\partial \theta} + \frac{u}{r}, & u_{zz} &= \frac{\partial w}{\partial z}, \\ 2u_{\theta z} &= \frac{1}{r} \frac{\partial w}{\partial \theta} + \frac{\partial v}{\partial z}, & 2u_{rz} &= \frac{\partial u}{\partial z} + \frac{\partial w}{\partial r}, & 2u_{r\theta} &= \frac{\partial v}{\partial r} - \frac{v}{r} + \frac{1}{r} \frac{\partial u}{\partial \theta}. \end{aligned} \quad (43)$$

From the elements of the stress tensor the characteristic amount of stress at a particular position can be given by the von Mises stress which satisfies

$$2\sigma_{\text{VM}}^2 = (\sigma_1 - \sigma_2)^2 + (\sigma_1 - \sigma_3)^2 + (\sigma_2 - \sigma_3)^2 \quad (44)$$

where  $\sigma_1, \sigma_2, \sigma_3$  are the eigenvalues of the stress tensor. Being a function of the eigenvalues, the von Mises stress is invariant under coordinate transformations. Expressions (41)-(44) form the fundamental equations of linear thermoelasticity in cylindrical coordinates.

In general, the set of equations are coupled and a numerical method will be needed to solve the displacements before thermal stress can be computed. However, it is instructive to consider the special case where the displacement occurs in one of the three directions, due to the nature of temperature variation. In the following, we will address the thermal stress that arises from temperature variation in the radial direction. We want to emphasize that this situation corresponds to a worst case scenario since in reality the stresses are related and the overall affect will be a combination of radial and axial temperature variation.

## 4.2 Thermal stress due to radial temperature variation

Assuming that the displacement vector is of the form  $\vec{u} = \langle u(r), 0, 0 \rangle$  and converting to non-dimensional units reduces the expression (42) to

$$\frac{\partial}{\partial r} \left[ \frac{1}{r} \frac{\partial}{\partial r} (ru) \right] = \epsilon \frac{(1+\nu)}{(1-\nu)} \frac{\partial \Theta_1}{\partial r}, \quad u(0) < \infty, \quad \sigma_{rr}(R) = 0.$$

Note that the stress has been non-dimensionalized by  $\alpha_0 \Delta T E / (1-\nu)$ . We have assumed here that  $\partial \Theta / \partial z \simeq 0$  since we want to focus on the sole effect of any radial temperature variations. The solution satisfying the boundary conditions is

$$u(r) = \epsilon \frac{(1+\nu)}{(1-\nu)} \left[ \frac{1}{r} \int_0^r \Theta_1(s) s ds + (1-2\nu) \frac{r}{R^2} \int_0^R \Theta_1(s) s ds \right]$$

and the corresponding nontrivial stresses are

$$\left. \begin{aligned} \sigma_{rr} &= \epsilon \left[ \frac{1}{R^2} \int_0^R \Theta_1(s) s ds - \frac{1}{r^2} \int_0^r \Theta_1(s) s ds \right], \\ \sigma_{\theta\theta} &= \epsilon \left[ \frac{1}{R^2} \int_0^R \Theta_1(s) s ds + \frac{1}{r^2} \int_0^r \Theta_1(s) s ds - \Theta_1(r) \right], \\ \sigma_{zz} &= \epsilon \left[ \frac{2}{R^2} \int_0^R \Theta_1(s) s ds - \Theta_1(r) \right] \end{aligned} \right\} \quad (45)$$

with  $\sigma_{zz}$  modified using St. Venant's principle.

From (30) we obtain

$$\sigma_{rr} = \frac{1}{4}\epsilon\Theta_1^1(z, t) (R(z)^2 - r^2), \quad \sigma_{\theta\theta} = \frac{1}{4}\epsilon\Theta_1^1(z, t) (R(z)^2 - 3r^2), \quad \sigma_{zz} = \frac{1}{2}\epsilon\Theta_1^1(z, t) (R(z)^2 - 2r^2). \quad (46)$$

Using (44) to compute the von Mises stress gives

$$\sigma_{\text{VM}} = -\frac{1}{4}\epsilon\Theta_1^1(z, t)R(z)^2 \left[ 1 - 4\left(\frac{r}{R(z)}\right)^2 + 7\left(\frac{r}{R(z)}\right)^4 \right]^{1/2}. \quad (47)$$

The object in the square brackets is a shape factor which ranges from a value of  $\sqrt{3/7}$  at a radius of  $r = \sqrt{3/7}R(z)$  to a maximum value of two at the outer edge of the crystal. For  $\sqrt{4/7}R(z) < r \leq R(z)$  this factor is greater than one.

In the pseudo-steady case  $\Theta_1^1$  is given by expression (31) and (26) so that equation (47) becomes

$$\sigma_{\text{VM}} = \frac{1}{16}\epsilon\Theta_{0,zz}R(z)^2 \left[ 1 - 4\left(\frac{r}{R(z)}\right)^2 + 7\left(\frac{r}{R(z)}\right)^4 \right]^{1/2} \quad (48)$$

indicating that the stress level is a characteristic of the concavity of the temperature in the axial direction. It should be noted that the stress is also linearly proportional to the Biot number  $\epsilon$ . This indicates that the an increase in the crystal radius will also increase the stress level, other conditions being equal. It also indicates that the increase of radius can be off-set by reducing the heat transfer coefficient  $h_{gs}$ , suggesting that a possible way for reducing the stress by changing the local heat flux from the crystal lateral surface.

As other stress, such as the total resolved stress is often considered more relevant for causing defects, it is important to point out that the same characteristic remains for different representation of the thermal stress, or the crystals being pulled in different directions, which will be the topic of the following two sections.

### 4.3 Resolved stress

InSb crystallizes in a zincblende or  $\bar{4}3m$  structure. The structure description is two interpenetrating face-centered cubic (f.c.c.) sublattices of In and Sb separated by the displacement vector  $a\langle 1, 1, 1 \rangle/4$ . Each In (Sb) atom is tetrahedrally coordinated with an Sb (In) atom. An alternative description of the structure is a f.c.c. sublattice of Sb atoms with one half of the tetrahedral sites filled with In atoms. The nearest neighbour distance is  $\sqrt{3}a/4$  and the lattice parameter is  $a = 0.6476$  nm.

The preferred method of dislocation generation in InSb, as in all III-V semiconductors, is through the generation of slip defects. In particular the  $\{111\}$ ,  $\langle 1\bar{1}0 \rangle$  slip system [3]. This system consists of four glide planes within which atoms can slip in one of three directions. For example, in the (111) plane the slip directions are  $[10\bar{1}]$ ,  $[\bar{1}10]$  and  $[0\bar{1}1]$ . Figure 4 looks down the  $z$ -axis of the tetrahedral structure of the crystal and shows each of the twelve permissible glide directions classified into five different categories.

The amount of stress in a particular slip direction  $\vec{g}$  within a given glide plane with normal  $\vec{n}$  is known as the resolved stress,  $\sigma_{\text{RS}}$ . If one assumes that the crystallographic axes coincide with the coordinate axes then  $\sigma_{\text{RS}}$  is computed by finding

$$\sigma_{\text{RS}} = \vec{g}^T Q \sigma Q^T \vec{n} \quad (49)$$

where  $Q$  is the coordinate transformation matrix that takes  $(r, \theta, z) \rightarrow (x, y, z)$  and  $\sigma$  is the stress tensor in the  $(r, \theta, z)$  coordinates:

$$Q = \begin{pmatrix} \cos \theta & \sin \theta & 0 \\ -\sin \theta & \cos \theta & 0 \\ 0 & 0 & 1 \end{pmatrix}, \quad \sigma = \begin{pmatrix} \sigma_{rr} & 0 & 0 \\ 0 & \sigma_{\theta\theta} & 0 \\ 0 & 0 & \sigma_{zz} \end{pmatrix}.$$

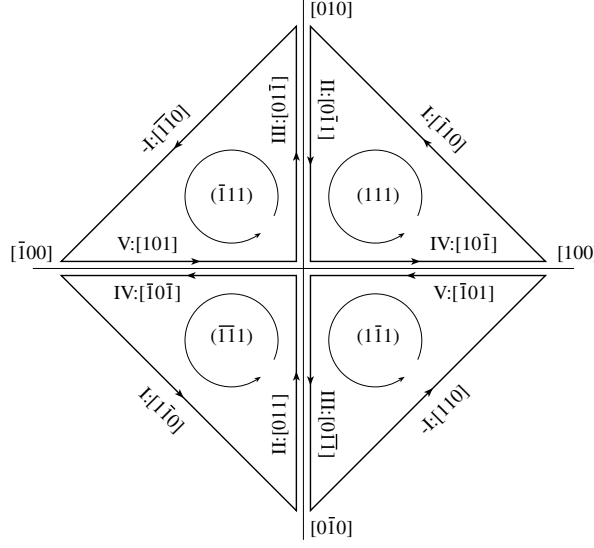


Figure 4: Illustrated are each of the twelve slip directions in the  $\{111\}$ ,  $\langle 1\bar{1}0 \rangle$  slip system. The roman numerals refer to the functional form of the stress in the direction of the appropriate slip plane.

For example, consider the stress in the (111) plane in the  $[\bar{1}10]$  direction. Using expression (49) yields

$$\begin{aligned} \sigma_{\text{RS}}^{\text{I}} &= \frac{1}{\sqrt{2}}(-1, 1, 0) \begin{pmatrix} \cos \theta & -\sin \theta & 0 \\ \sin \theta & \cos \theta & 0 \\ 0 & 0 & 1 \end{pmatrix} \begin{pmatrix} \sigma_{rr} & 0 & 0 \\ 0 & \sigma_{\theta\theta} & 0 \\ 0 & 0 & \sigma_{zz} \end{pmatrix} \begin{pmatrix} \cos \theta & \sin \theta & 0 \\ -\sin \theta & \cos \theta & 0 \\ 0 & 0 & 1 \end{pmatrix} \frac{1}{\sqrt{3}} \begin{pmatrix} 1 \\ 1 \\ 1 \end{pmatrix} \\ &= -\frac{1}{\sqrt{6}}(\sigma_{rr} - \sigma_{\theta\theta}) \cos 2\theta. \end{aligned}$$

Summarizing the five categories as classified in Figure 4 yields<sup>2</sup>

$$\left. \begin{aligned} \sigma_{\text{RS}}^{\text{I}} &= -\frac{1}{\sqrt{6}}(\sigma_{rr} - \sigma_{\theta\theta}) \cos 2\theta, \\ \sigma_{\text{RS}}^{\text{II}} &= \frac{1}{\sqrt{6}}[(\sigma_{zz} - \sigma_{\theta\theta}) - (\sigma_{rr} - \sigma_{\theta\theta})(\sin^2 \theta + \sin \theta \cos \theta)], \\ \sigma_{\text{RS}}^{\text{III}} &= \frac{1}{\sqrt{6}}[-(\sigma_{zz} - \sigma_{\theta\theta}) + (\sigma_{rr} - \sigma_{\theta\theta})(\sin^2 \theta - \sin \theta \cos \theta)], \\ \sigma_{\text{RS}}^{\text{IV}} &= \frac{1}{\sqrt{6}}[-(\sigma_{zz} - \sigma_{\theta\theta}) + (\sigma_{rr} - \sigma_{\theta\theta})(\cos^2 \theta + \sin \theta \cos \theta)], \\ \sigma_{\text{RS}}^{\text{V}} &= \frac{1}{\sqrt{6}}[(\sigma_{zz} - \sigma_{\theta\theta}) - (\sigma_{rr} - \sigma_{\theta\theta})(\cos^2 \theta - \sin \theta \cos \theta)]. \end{aligned} \right\} \quad (50)$$

Plastic deformation of the crystal occurs if the stress in any of the twelve slip directions exceeds the critical resolved shear stress,  $\sigma_{\text{crss}}$ . To first order, the actual density of dislocations suffered by the crystal is proportional to the total excess stress at any given point within the crystal. In this sense, an estimation of where dislocations are likely to occur is given by the distribution of the total absolute stress given by

$$|\sigma_{\text{TOT}}| = 4|\sigma_{\text{RS}}^{\text{I}}| + 2(|\sigma_{\text{RS}}^{\text{II}}| + |\sigma_{\text{RS}}^{\text{III}}| + |\sigma_{\text{RS}}^{\text{IV}}| + |\sigma_{\text{RS}}^{\text{V}}|).$$

An additional complication is that in general, the elastic constants depend on the pulling direction since the thermal and crystallographic axes are not aligned. However, for crystals that belong to the cubic classes this effect does not play a role [1].

<sup>2</sup>Note that  $\theta = -\varphi$  where  $\varphi$  is the angular coordinate used by Jordan et al. [3].

#### 4.4 Crystal extraction in an arbitrary direction

The previous subsection supposes that the crystal is extracted from the melt in a direction coincident with the crystallographic axes. To consider a misalignment in these coordinate systems, let  $(\mathbf{i}, \mathbf{j}, \mathbf{k})$  denote a frame with its  $z$ -axis coincident with the pulling direction and  $(\mathbf{i}', \mathbf{j}', \mathbf{k}')$  denote a frame coincident with the crystallographic axes. In the  $(\mathbf{i}, \mathbf{j}, \mathbf{k})$  frame we need to represent  $\vec{n}$  and  $\vec{g}$ , the normal vector to the stress plane and the glide direction, in the unprimed coordinates. These direction must change because they are with respect to the crystallographic axes which is no longer the unprimed frame. This is easily remedied with a coordinate transformation  $U_{v_p}$  depending on the pulling direction which takes vectors in the primed frame to the unprimed frame. If one denotes the rows of  $U_{v_p}$  as  $\hat{r}_1$ ,  $\hat{r}_2$  and  $\hat{r}_3$  then possible representation would be to let  $\vec{r}_3 = \vec{v}_p$ ,  $\vec{r}_2 = \mathbf{j} - \mathbf{j}\vec{v}_p^T\vec{v}_p/\|\vec{v}_p\|^2$ ,  $\vec{r}_1 = \vec{r}_2 \times \vec{r}_3$  and then computing the unit vectors. For example, if one pulls in the  $[111]$  direction a possible representation for  $U_{v_p}$  is

$$U_{[111]} = \begin{pmatrix} \frac{1}{\sqrt{2}} & 0 & -\frac{1}{\sqrt{2}} \\ -\frac{1}{\sqrt{6}} & \frac{2}{\sqrt{6}} & -\frac{1}{\sqrt{6}} \\ \frac{1}{\sqrt{3}} & \frac{1}{\sqrt{3}} & \frac{1}{\sqrt{3}} \end{pmatrix}.$$

As a result, expression (49) must be modified to

$$\sigma_{RS} = \vec{g}^T U_{v_p}^T Q \sigma Q^T U_{v_p} \vec{n}. \quad (51)$$

Another difficulty when pulling in an arbitrary direction is that in general the symmetry of the five classes of resolved shear stress will be broken. As a result,

$$|\sigma_{TOT}| = \sum_{i=1}^{12} |\sigma_{RS}^i| \quad (52)$$

where the twelve indices correspond to the twelve different  $\vec{g}$ ,  $\vec{n}$  combinations that project the pulling direction into each element of the  $\{111\}$ ,  $\langle 1\bar{1}0 \rangle$  slip system.

## 5 Numerical Results and Discussion

We now present some typical numerical results obtained using the formula derived earlier. We first discuss the temperature solutions for the decoupled growth, i.e., the heat flux from the melt to the crystal is assumed a known (constant) value. In particular, we compare the pseudo-steady and the unsteady solution. Even though the Stefan number is not much bigger than unity, the results show that the pseudo-steady solutions are in good agreement with the unsteady calculation. This indicates that the thermal stress can be computed using the pseudo-steady solution, which greatly simplifies the calculation. The case for coupled growth is also investigated and we show that the transient effect in the melt is only important towards the end of the growth. During the growth, the heat flux from the melt to the crystal changes slowly, suggesting that the temperature solutions for the decoupled case are good approximations. The thermal stress is computed based on the pseudo-steady solution using decoupled growth condition for simplicity.

### 5.1 Temperature solutions

Table 2 displays the various quantities used in the simulation and not found in the previous table. The crucible shape is given as  $z = r^b$ ,  $b \geq 1$  where  $r$  and  $z$  are non-dimensionalized by  $\bar{R}_c$  and  $\bar{H}_c$ . The seed radius refers to the solution for the cone. For the case of the cylinder the seed radius is the same as the mean radius.

Data	Symbol	Value
Growing Properties		
Ambient temperature	$T_a$	600 K
Seed radius	$R_{seed}$	0.005 m
Seed length	$Z_{seed}$	0.03 m
Crucible depth	$\bar{H}_c$	0.0875 m
Crucible radius	$\bar{R}_c$	0.0875 m
Thermal expansion	$\alpha_0$	$5.5 \times 10^{-6}$ /K
Liquid Properties		
Density	$\rho_l$	$6.47 \times 10^3$ kg/m <sup>3</sup>
Thermal Conductivity	$k_l$	9.23 W/m K
Heat Capacity	$\rho_l c_l$	$1.7 \times 10^6$ J/m <sup>3</sup> K
Heat Transfer Coefficients		
Crystal-Liquid	$h_{sl}$	3700 W/m <sup>2</sup> K
Gas-Liquid	$h_{gl}$	2 W/m <sup>2</sup> K
Crucible-Liquid	$h_{cl}$	2470 W/m <sup>2</sup> K

Table 2: Remaining liquid and growth parameters used in the simulations. The values of the heat transfer coefficients  $h_{sl}$  and  $h_{cl}$  are based on estimated boundary layer thickness due to Ekman layer (rotations of crucible and the crystal at 5 rpm) and natural convection (Grashof's number  $\simeq 2.0 \times 10^5$  and Reynolds number  $\simeq 550$ ).

### 5.1.1 Decoupled growth

To begin we assume as a worst case scenario that  $\gamma = 0$  so that the melt in the crucible is essentially decoupled from the crystal we attempt to justify that the growth of the crystal is pseudo-steady. Figure 5 illustrates the time dependent growth of the position of the solidus,  $S_0(t)$ , for a cylindrical and a conical crystal. For each situation,  $\epsilon_1$  corresponds to  $h_{gs} = 1$  and  $\epsilon_2$  corresponds to  $h_{gs} = 4$  in expression (6). Note that the solutions are also applicable to different conditions. For example, the results for  $\epsilon_2$  can also be viewed as a combination of  $h_{gs} = 1$  and  $\bar{R} = 0.12$  meters. This pseudo-steady behaviour is also observed for the first order perturbation. Figure 6 shows the radial dependence of the crystal at the end of the growth cycle. In both the case of a cylindrical and a conical crystal the growth interface is convex (viewed from inside the crystal). For the conical crystal the interface is flatter even though the curvature grows with time for both cases.

The temperature contours are plotted in Figures 7 & 8 for the cylindrical and conical crystals respectively. It can be seen that the pseudo-steady and unsteady solutions are in close agreement. The temperature gradients are larger for larger values of  $\epsilon$ , as suggested by the formulas derived earlier. The implication on thermal stress will be discussed in Section 5.2.

### 5.1.2 Coupled growth with melt in the crucible

We focus on the possible transient effect of the crucible temperature on the growth. We are interested in the pulling rate,  $v_p$ ; the heat flux from the melt to the crystal,  $\gamma$  and the melt temperature itself,  $T_l$ . For simplicity, only results for the cylindrical case are presented. Initially we set the crystal temperature distribution to be that given by the solution for the pseudo-steady model (27) with  $S_0 = Z_{seed}$  and  $\delta = 0$ . As well, the initial melt temperature was taken to be 0.05 K and 0.075 K above  $T_s$  and the crucible temperature was chosen to be  $T_c = 0.118$  K and 0.141 K above the melting temperature so that the melt pool inside the crucible is close to thermal equilibrium.

In Figure 9, we have plotted the non-dimensional melt temperature  $T_l$ , heat flux from melt to the crystal  $\gamma$  as well as the displacement of the interfaces for crystal/melt  $S_0$  and melt/gas  $u_w$ , using  $T_c = 0.118$  K and

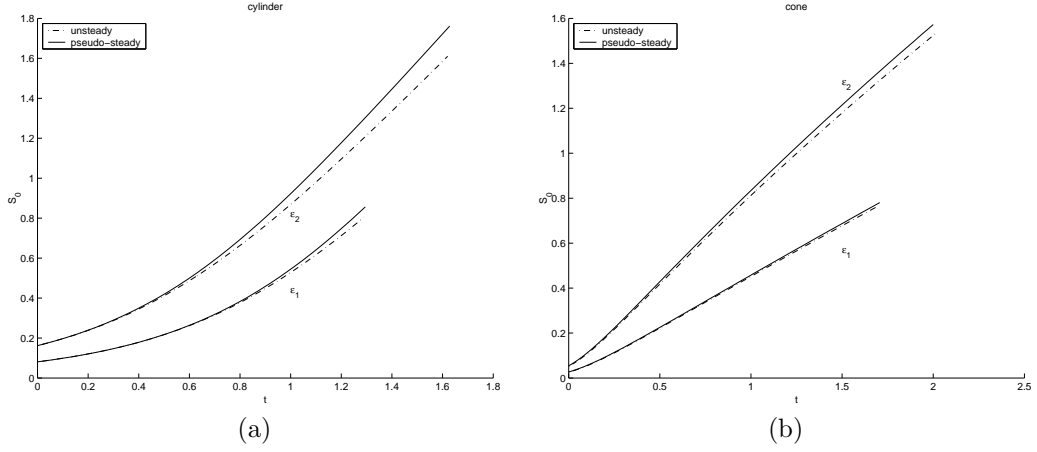


Figure 5: Comparison of  $S_0$  as a function of time for the cylinder and the cone.

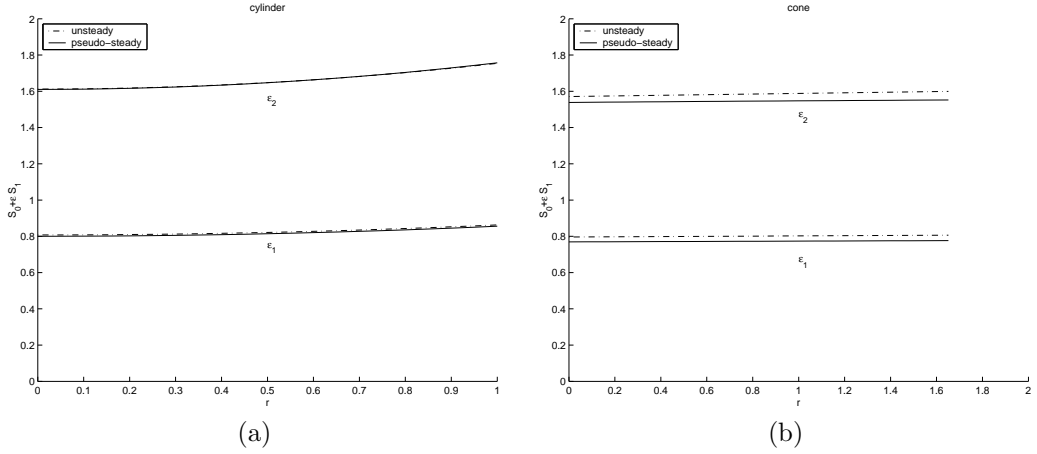


Figure 6:  $S = S_0 + \epsilon S_1$  for various  $\epsilon$  at the final time.

0.141 K above  $T_s$ . It can be seen that for these choice of the parameters, the small amount of heat flux  $\gamma$  slows the initial growth. As a result, it takes much longer for the crystal to reach the final length. However, the value of  $\gamma$  and  $T_l$  do not change dramatically over the growth period, indicating a stable growth.

## 5.2 Thermal stress

For an anisotropic crystal the values of  $E$  and  $\nu$  depend on the direction the stress occurs. However, we are only interested in the resolved stress in the slip-strain system and crystals that belong any of the cubic classes these values are invariant [1]. For InSb one has

$$E_{\{111\}} = \frac{4(C_{11} + 2C_{12})(C_{11} - C_{12})C_{44}}{(C_{11} + 2C_{12})(C_{11} - C_{12}) + 2C_{11}C_{44}} = 6.18 \times 10^4 \text{ MPa},$$

$$\nu_{\{111\}} = \frac{1}{3} \frac{(C_{11} + 2C_{12})(C_{11} - C_{12}) - 2C_{44}(C_{11} - 4C_{12})}{(C_{11} + 2C_{12})(C_{11} - C_{12}) + 2C_{11}C_{44}} = 0.364$$

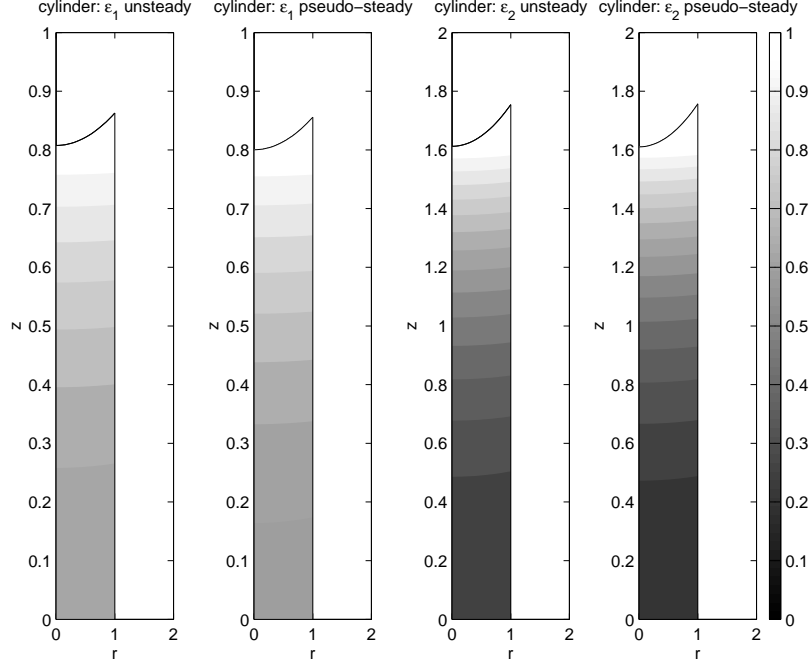


Figure 7: Non-dimensional temperature contours cylinder at the end of the growth.

where  $C_{11} = 6.70 \times 10^4$ ,  $C_{12} = 3.65 \times 10^4$ ,  $C_{44} = 3.02 \times 10^4$  are crystal stiffnesses in MPa and consequently

$$\frac{E}{1 - \nu} \Big|_{\{111\}} = \frac{4(C_{11} + 2C_{12})C_{44}}{C_{11} + 2C_{12} + 4C_{44}} = 9.72 \times 10^4 \text{ MPa}. \quad (53)$$

As a result, the dimensional constant for the stress calculations is  $\alpha_0 \Delta T E / (1 - \nu) \simeq 106 \text{ MPa}$ .

Figure 10 shows the stress contours of the von Mises stress in units of MPa for the cylinder and the cone at the end of the growth. For a fixed value of  $\epsilon$  the stress in the conical case is about one-half that of the cylindrical case. Also, increasing  $\epsilon$  increases the stress level dramatically. By growing a conical crystal the stress can be reduced significantly. For a given temperature the amount of stress at which crystal deformation begins to occur is known as the critical resolved shear stress,  $\sigma_{\text{crss}}$ . In the case of InSb,  $\sigma_{\text{crss}}$  varies from 0.245 MPa [5] to 4.90 MPa [2] as the temperature varies from  $T_s = 798.4 \text{ K}$  to 491 K respectively indicating that the conical crystal remains below this critical stress level.

An additional method of reducing the stress level in the crystal is to use the anisotropic nature of the crystal to our advantage by changing the direction in which the crystal is pulled. From expressions (51) and (52) one can see that for a fixed vertical position in the crystal the total absolute resolved stress is a complicated function of the angular coordinate. Figure 11 shows the stress pattern for a cylindrical crystal just inside the crystal-melt interface when the crystal is pulled in the directions [001], [111], and [211] respectively. The [211] direction is a preferred growth direction [6] and the other two directions are for comparative purposes. Notice that the isostress contours are square for the [001] direction and hexagonal for the [111] direction while the [211] direction generates distorted rectangular isostress curves. If one assumes that the crystal will solidify in a manner consistent with minimizing the surface stress then these curves should somewhat approximate the actual cross-sectional shape of the crystal as it is pulled from the melt. Although changing the pulling direction does have a small bearing on the total amount of stress, these variations are small compared  $\epsilon$  variation. Changing the pulling direction is much more effective in redistributing the stress within a particular cross section. One final complication is that not all growth directions are amenable to

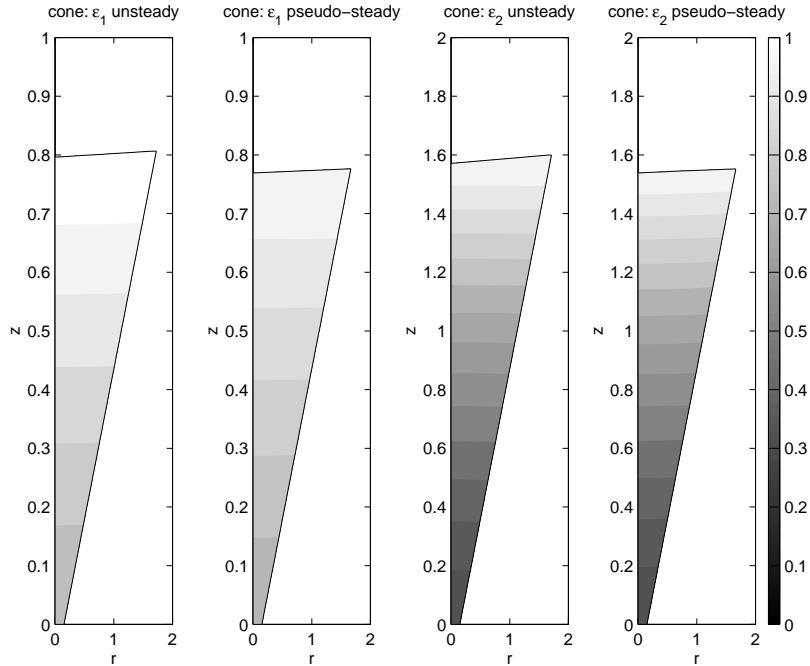


Figure 8: Non-dimensional temperature contours for the cone at the end of the growth.

crystal growth [6]. We plan to address the issue of optimizing the growth direction in a subsequent paper.

## 6 Conclusion

In this study, we present a semi-analytical approach for the temperature and thermal stress inside an InSb crystal. An important feature of the approach is that it allows us to derive explicit relationship between the thermal stress and relevant physical and geometrical parameters. This is achieved by using asymptotic expansion of the solution in the Biot number, characterizing the lateral heat flux. The asymptotic solution is obtained by solving essentially one-dimensional problems. The results show that the stress induced by radial temperature variation is related to the size of the crystal (radius) and heat flux through the side surface. On the other hand, the effect of the crystal radius on the stress induced by the axial temperature variation is much weaker. The heat flux through the side surface is an important factor for reducing the overall thermal stress inside the crystal.

The other advantages of our semi-analytical approach is that it can be extended to cases with more complicated models for the melt and gas flows. For example, the effect of the gas flow on the lateral heat flux between the crystal surface and the gas can be modelled by a non-constant heat exchange coefficient  $h_{gs}$ . The motion of the melt can also be modelled by a similar approach, using a boundary layer argument [25]. These will be the subject of a subsequent paper.

As pointed earlier, we have assumed that the pulling rate can be adjusted to grow a crystal with desirable shape. In practice, this may not be easy to achieve. Models and computations have been carried out to capture the motion of the three-phase contact point [9, 24], which can be incorporated with the current model in a straightforward fashion. This work is currently underway.

Finally, we note that we have not discussed the validity of the plane strain assumption. We believe that an asymptotic argument similar to that used for the temperature can be employed to derive the plane strain solution as part of the asymptotic series. We plan to address this issue also in a subsequent paper.

**Acknowledgement.** The authors wish to thank Firebird Semiconductors Inc., the Mathematics of Information Technology and Complex Systems (MITACS), a Network of Centers of Excellence and the Nature Sciences and Engineering Research Council (NSERC) of Canada for their financial support.

## References

- [1] Brantley, W.A., (1973). *Calculated elastic constraints for stress problems associated with semiconductor devices*, Journal of Applied Physics, 44(1), pp. 534-535.
- [2] Chaudhuri, A.R., Patel, J.R. & Rubin, L.G., (1962). Velocities and Densities of Dislocations in Germanium and Other Semiconductor Crystals. *Journal of Applied Physics*, 33, pp. 2736-2746.
- [3] Jordan, A.S., Caruso, R. & von Neida, A.R., (1980). *A Thermoelastic Analysis of Dislocation Generation in Pulled GaAs Crystals*, The Bell System Technical Journal, 59(4), pp. 593-637.
- [4] Landau, L.D., Lifshitz, E.M., (1970). *Theory of Elasticity*, 2nd ed. Pergamon Press: Oxford.
- [5] Mil'vidskii, M.G. & Bochkarev, E.P., (1978). Creation of defects during the growth of semiconductor single crystals and films. *Journal of Crystal Growth*, 44(1), pp. 61-74.
- [6] Micklethwaite, W.F., Firebird Semiconductors Ltd., personal communication.
- [7] Nowinski, J.L., (1978). *Theory of Thermoelasticity with applications*. Sijthoff & Noordhoff International Publishers Alphen aan den Rijn: The Netherlands.
- [8] Somewhere that states that thermal stress gives rise to defects. (Experimental) Get a Physical Review paper.
- [9] Tatachenko, Y.A., (1993). *Shaped Crystal Growth*. Kluwer Academic Publishers, Boston.
- [10] Sinno, T., Dornberg, E., von Ammon, W., Brown, R.A. and Dupret, F., (2002). Defect Engineering of Czochralski Single-Crystal Silicon. *Material Science and Engineering Reports*, 28, pp. 149-198.
- [11] Tanahasji, K., Kikuchi, M., Higashino, T., Inoue, N. and Mizokawa, Y. (2000). Concentration of Point Defects Changed by Thermal Stress in Growing CZ Silicon Crystal: Effect of the Growth Rate. *Journal of Crystal Growth*, 210, pp. 45-48.
- [12] Gulluoglu, A.N. and Tsai, C.T. (1999). Effect of Growth Parameters on Dislocation Generation in InP Single Crystal Grown by the Vertical Gradient Freeze Process. *Acta Mater.*, 47(8), pp. 2313-2322.
- [13] Alexander, H. and Hassen, P. (1968). Dislocation and Plastic Flow in the Diamond Structure. *Solid State Phys.*, 22, pp. 27-158.
- [14] Dupret, F. and van den Bogaert, N. (1994). Modeling Bridgeman and Czochralski Growth. In *Handbook of Crystal Growth*, 2B, Chapter 15, Hurle, D.T.J. ed., North-Holland. Amsterdam.
- [15] Brown, R.A., (1988). Transport Process in Czochralski Growth. *AIChE J.*, 34, pp. .
- [16] Chan, Y.T., Gilbeling, H.J. and Grubin, H.L. (1988). Numerical Simulation of the Czochralski Growth. *J. Appl. Phys.*, 64, pp. 1425-1439.
- [17] Hurle, D.T.J. (1994). *Handbook of Crystal Growth*, 1 & 2, North-Holland. Amsterdam.
- [18] Hurle, D.T.J. (1993). *Crystal Pulling from the Melt*, Springer-Verlag, Berlin.
- [19] Muller, G. (2002). Experimental Analysis and Modeling of MGGrowth Processes. *J. Crystal Growth*, 237-239, pp. 1628-1637.

- [20] Muller, G. (1988). Convection and Inhomogeneities in Crystal Growth from Melt. In Crystals, 12 (Freyhardt, F.C. ed.), Springer-Verlag, Berlin.
- [21] Prasad, V., Zhang, H. and Anselmo, A. (1997). Transport Phenomena in Czochralski Crystal Growth Process. *Advances in Heat Transfer*, 30, pp. 313-435.
- [22] Volkl, J. (1994). Stress Computation in Czochralski. In Handbook of Crystal Growth, 2B, Chapter 14, Hurle, D.T.J. ed., North-Holland. Amesterdam.
- [23] Derby, J.J. and Brown, R.A. (1988). On the Quasi-Steady-State Assumption in MOdeling Czochralski Crystal Growth. *J. Crystal Growth*, 87, pp. 251-260.
- [24] Crowley, A.B. (1983). Mathematical Modeling of Heat Flow in Czochralski Crystal Pulling. *IMA J. Appl. Math.*, 30, pp. 173-189.
- [25] Need from Ian.

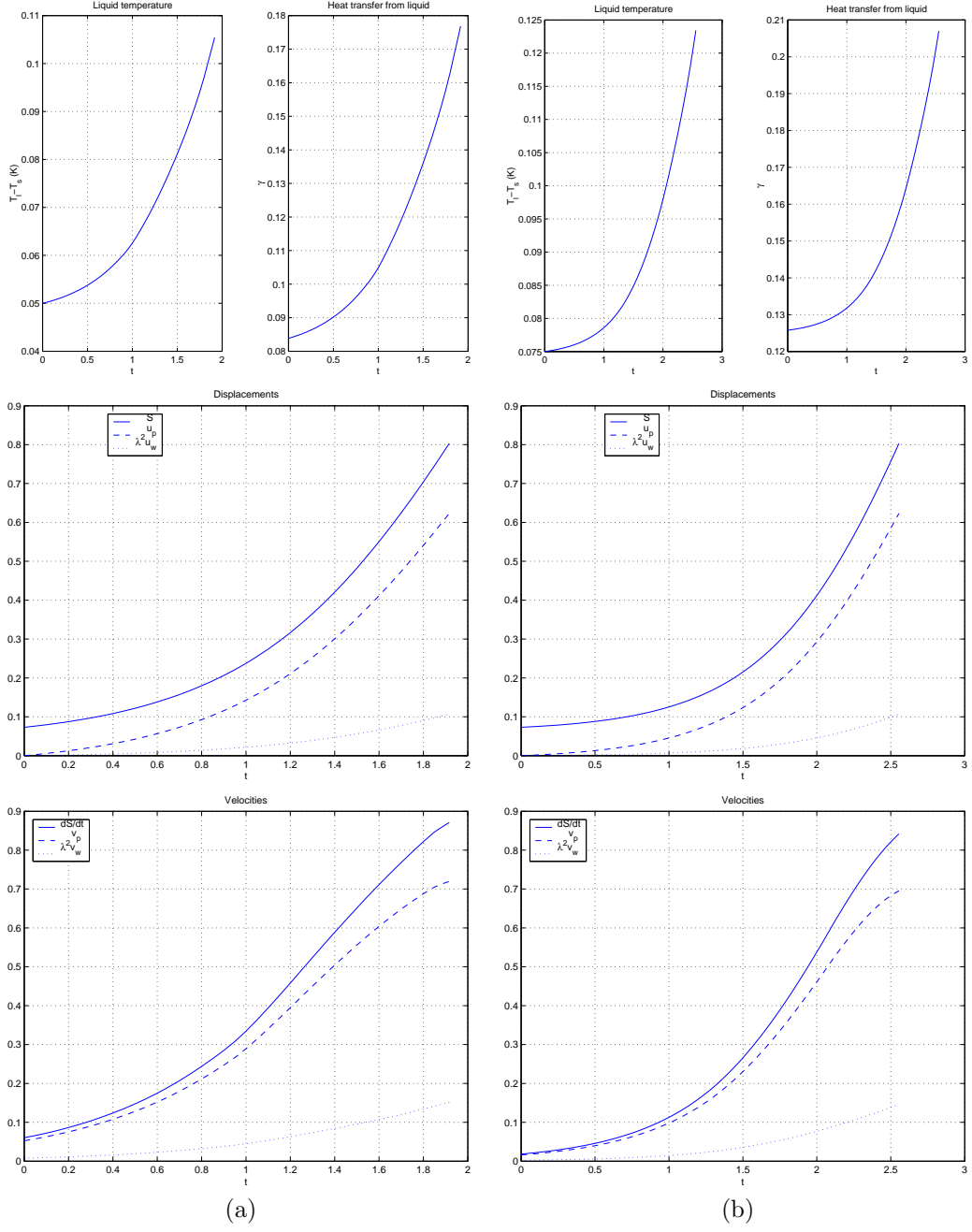


Figure 9: Coupled growth (a)  $T_c = 0.118$  K and (b)  $T_c = 0.141$  K. Plotted are (from top to bottom) melt temperature and heat flux  $\gamma$ , displacements and interface speeds and pulling rate.

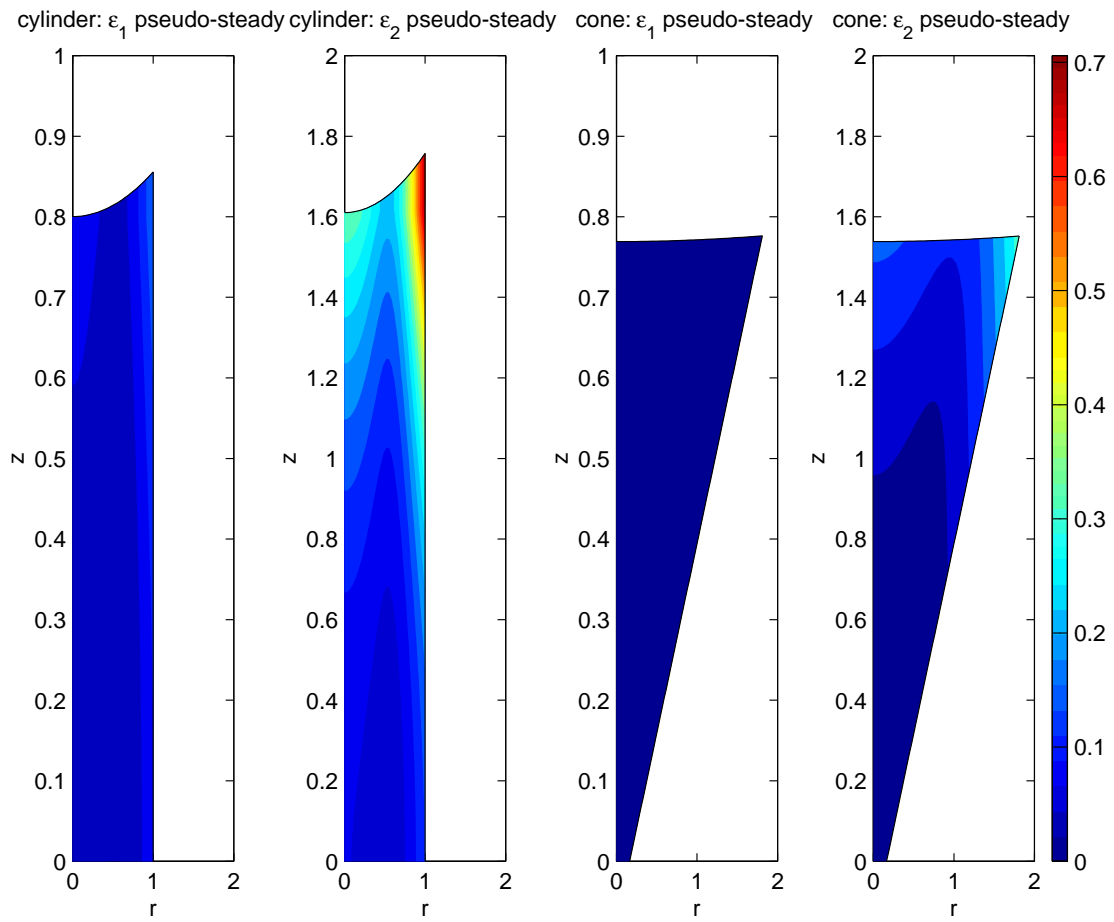


Figure 10: von Mises stress in MPa for the cylindrical and conical crystal cases.